The Role of Gas Pressure and Lateral Stress on Blistering

W.G. Wolfer

April 1980

UWFDM-347

J. Nucl. Matls. 93 & 94, 713-730 (1980).

FUSION TECHNOLOGY INSTITUTE

UNIVERSITY OF WISCONSIN

MADISON WISCONSIN

The Role of Gas Pressure and Lateral Stress on Blistering

W.G. Wolfer

Fusion Technology Institute
University of Wisconsin
1500 Engineering Drive
Madison, WI 53706

http://fti.neep.wisc.edu

April 1980

UWFDM-347

J. Nucl. Matls. 93 & 94, 713-730 (1980).

The Role of Gas Pressure and Lateral Stress on Blistering

W. G. Wolfer

Fusion Engineering Program
Nuclear Engineering Department
University of Wisconsin
Madison WI 53706 U.S.A.

April 1980

UWFDM-347

Paper presented at the 4th International Conference on Plasma Surface Interactions in Controlled Fusion Devices, Garmisch-Partenkirchen, Federal Republic of Germany, April 1980.

Abstract

Both gas pressure in bubbles and lateral stress have been suggested as primary causes of blistering. An analysis of both mechanisms is presented, and the conditions for blistering are examined. To realistically predict the gas pressure in bubbles, a recently derived high-density equation of state for helium is utilized.

It is shown that the formation of overpressurized gas bubbles leads to a state of stress in the surface layer which is a superposition of a tensile microstress surrounding the bubbles and a lateral compressive macrostress across the bombarded layer. When the microstress reaches a value of 0.003 μ for fcc metals or 0.009 μ for bcc metals, interbubble fracture occurs. These critical values are reached for an implanted helium concentration between 20 to 40%. The exact value depends to some degree on the bubble density, the temperature, and the helium to vacancy ratio.

The lateral stress is shown to saturate prior to the onset of blistering, but it remains the driving force for blister dome formation once a sufficiently large area of the bombarded layer is detached.

I. Introduction

Several mechanisms have been proposed to explain the occurrence of blistering when inert gases are implanted into solids. A review of these mechanisms and of the experimental observations has been given by Das and Kaminsky [1] and more recently by Scherzer et al. [2].

Three fundamentally different causes have been suggested for blistering: formation of an interconnected network of inert gas atoms within the host crystal; failure of the material surrounding overpressurized gas bubbles; and buckling of the bombarded layer under large lateral stresses produced by swelling.

At temperatures where point defects are mobile which have been produced by the concomitant radiation damage, the inert gas atoms are also believed to migrate. It has been shown [3] by computer simulation studies that helium atoms forming half of a mixed interstitial dumbbell are highly mobile even at moderate temperatures. In any case, numerous studies have confirmed the existence of small bubbles, so that the percolation model of an interconnected network of gas atoms, as advanced by Wilson et al. [4], is no longer considered as the ultimate cause of blistering.

However, the other two mechanisms, the gas-driven and the stress-driven, are still viewed as competing explanations. It is the purpose of this paper to analyse both mechanisms in more quantitative terms, and thereby elucidate the role of both overpressurized gas bubbles and lateral stresses. The outcome of the present analysis is that the pressurized gas bubbles are responsible for the decohesion of the bombarded layer from the underlying material, whereas the lateral stresses are the driving force for the appearance of dome-shaped blisters.

In the gas-driven model, as particularly championed by Evans [5], the gas pressure in bubbles is thought to exceed not only the surface tension, but the fracture strength of the surrounding material between bubbles. However, Evans bases his analysis on a very large value of the fracture stress, about 0.06 μ (where μ is the shear modulus), and an empirical gas law extrapolated way beyond its data-supported density range.

The quantitative results,and hence the viability of the gas-driven model, depend to a large degree on a reliable high-density equation of state. Accordingly, we have recently derived an equation of state for helium based on its interatomic potential and the very successful liquid state theories developed over the last decade. Although the details of this derivation are reported elsewhere [6], the pertinent results are summarized in Section II. This new equation of state for helium is applied in Section III to the interbubble fracture model.

In the stress-driven model, suggested by Behrisch et al. [7] and by EerNisse and Picraux [8], blister formation is seen as a buckling phenomenon of the bombarded layer in response to large lateral stresses. These compressive stresses are caused by swelling and the lateral restraint imposed by the underlying material. The implicit assumption in this model is that the lateral stresses build up steadily until a maximum value is reached at which point the layer buckles, thereby relaxing the lateral stresses. However, relaxation of the lateral stresses must occur continuously, and certainly long before the onset of blistering. The reason for this is simply that only small amounts of swelling, of the order of perhaps 0.2%, can be accommodated by an elastic compression. Yet very large amounts of swelling have been measured recently [9,10] prior to the onset of blistering. It must therefore be concluded that plastic deformation or

irradiation creep accompanies swelling. As shown by Wolfer and Garner [11], and discussed further in Section IV, this leads to an early saturation of the lateral stress prior to the onset of blistering. The combined role of stresses produced by overpressurized bubbles and swelling is finally analysed in Section V.

II. The High-Density Equation of State for Helium

Empirical equations of state for gaseous helium are restricted to pressures below 100 MPa [12]. Any extrapolation to pressures an order of magnitude higher, as required for small gas bubbles in solids, is suspect. Accordingly, an equation of state for helium in the gas phase was recently derived [6], utilizing the interatomic potential for helium as found by Beck [13], and the highly accurate liquid state theory as developed by Barker and Henderson [14], Anderson, Chandler, and Weeks [15], and further refined by Verlet and Weis [16]. This theory is also applicable to dense gases. It is based on a perturbation method, starting with a hard-sphere gas as a zero-order approximation. The effective hard-sphere diameter, d, of the atoms is selected such that the higher-order approximations are of lesser importance. It has been shown [14,15,16] that this approach leads to excellent results for the equation of state. The effective hard-sphere diameter, d, becomes a function of the temperature and density, because the actual interatomic potential is in fact soft.

Using this perturbation theory to first order, the equation of state of helium, expressed in terms of

$$z = \frac{p}{\rho k T} \tag{1}$$

was obtained [6] as shown in Fig. 1. Here, p is the gas pressure, k the Boltzmann constant, T the absolute temperature, and

$$\rho = m/n = \text{number of gas atoms/number of vacancies in one bubble,} \quad (2)$$

is the gas density. For our application, ρ is also expressed in terms of helium atoms per vacancy.

The equation of state is plotted as a function of various density measures used in the literature: the hard-sphere packing fraction

$$\eta_o = \frac{\pi}{6} d_o^3 \rho \quad (3)$$

where $d_o = 0.2637$ nm is the distance where the interatomic potential is zero; the reduced density $\rho^* = \rho\, d_o^3$; and the fraction of the liquid state density,

$$\eta_\ell = \frac{\pi}{6} R_m^2 \rho \quad , \quad (4)$$

where $R_m = 0.2969$ nm is the equilibrium interatomic distance.

Our theoretical equation of state is in good agreement with experimental data, i.e., for $\rho^* < 0.3$ and $z < 1.4$.

Due to the softness of the repulsive part of the interatomic potential, the effective hard-sphere diameter, d, and hence z, decrease with increasing temperature for a constant density ρ. Furthermore, z and the pressure p remain finite as the density approaches either the liquid density or a complete hexagonally closed-packed arrangement at $\eta_o^{max} = 0.7405$. In contrast, a simple van der Waals gas law with a fixed atomic diameter would result in a temperature independent z and an infinite pressure for the maximum packing fraction η_o^{max}. It is interesting to note that the helium density at η_o^{max} is equal to $6.06 \times 10^{22} cm^{-3}$, i.e., 89.5% of the metal atom

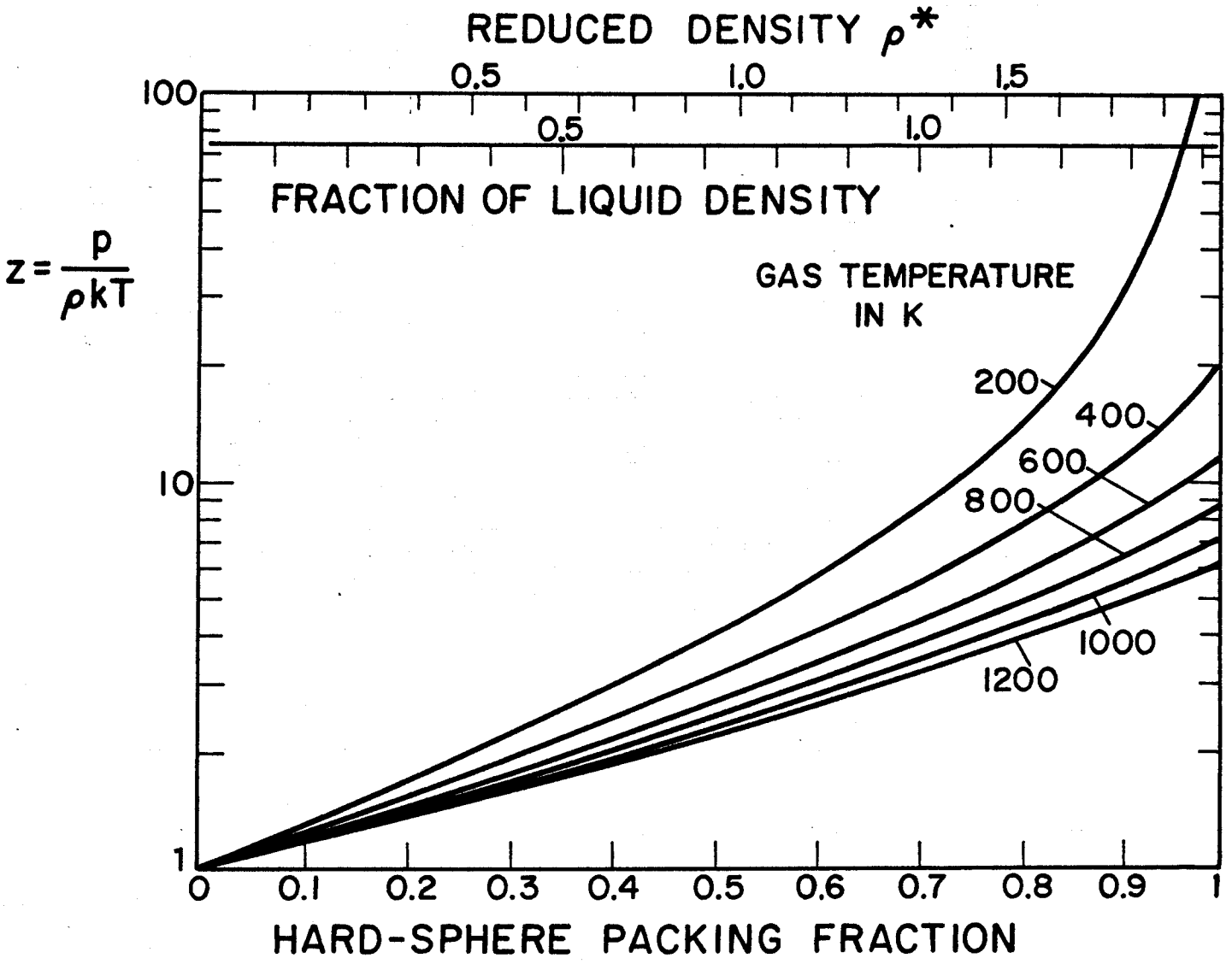

Fig. 1. Equation of state for gaseous helium.

density for nickel. At the onset of blistering, the helium/metal atom ratio is about 0.3. Therefore, inside the bubbles the helium density approaches the metal atom density, and may in fact exceed the value for n_o^{max}.

III. Stresses Produced by Overpressurized Gas Bubbles

An equilibrium bubble of radius r produces no elastic deformation in the surrounding material, as the gas pressure p inside is exactly balanced by the surface tension, $2\gamma/r$. Here, γ is the surface energy. For a non-equilibrium bubble, however, stresses are induced in the surrounding material such that

$$p - \frac{2\gamma}{r} = \sigma_r \tag{5}$$

where σ_r is the stress normal to the bubble surface. Furthermore, γ is now the surface stress rather than the surface energy. Although this distinction is important from a conceptual point of view, for practical purposes both are numerically of the same order. Experimental evidence seems to indicate [17] that the surface stress is less than the surface energy. It will be seen that our conclusions with regard to blistering are insensitive to the exact choice of the surface stress γ, and a typical value of 1 J/m^2 will suffice. Equation (5) serves as a boundary condition if the detailed stress distribution in the material is to be computed around each bubble. Needless to say, we are only interested in average values of the stresses between bubbles. They can be obtained in a simple manner by referring to Fig. 2.

We imagine an intersection cut of the material and the bubbles at any desired location. If the intersection plane is parallel to the surface, then the overall balance of forces along the cut requires that

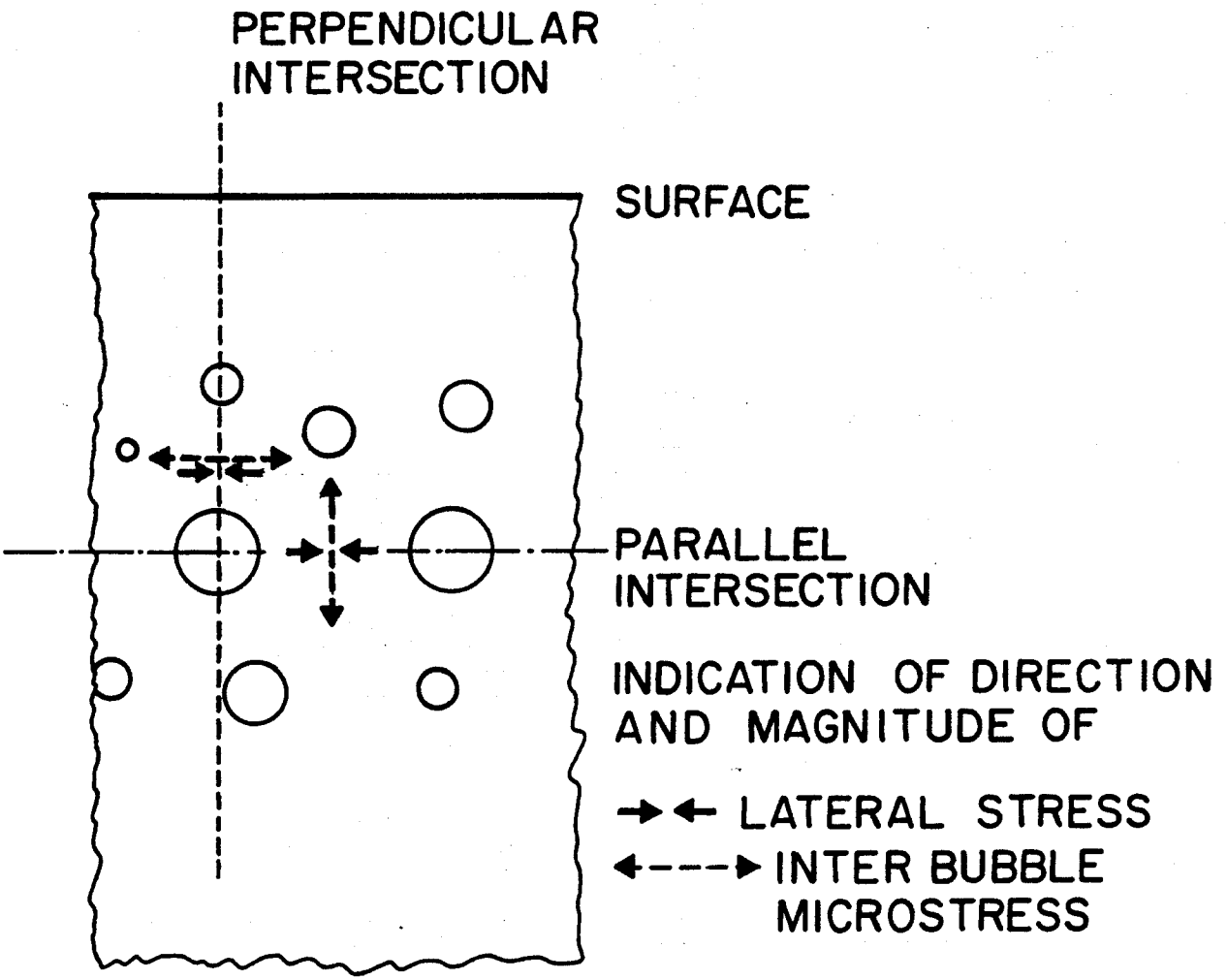

Fig. 2. Schematic cross section of the bombarded layer with gas bubbles and definitions of the lateral stress and interbubble microstress.

$$A(p - \frac{2\gamma}{r}) = (1 - A)\bar{\sigma}_n \quad . \tag{6}$$

This equation was given previously by Evans [5].

Here, A is fraction of the area intersected by bubbles, and $\bar{\sigma}_n$ is an average value for the microstress field between bubbles.

If we place the intersection perpendicular to the surface, as indicated by the dotted line in Fig. 2, we must include the lateral stress σ_L in the balance equation, so that

$$\sigma_L + A\ (p - \frac{2}{r}) = (1 - A)\ \bar{\sigma}_n \quad . \tag{7}$$

Note that the lateral stress σ_L is obtained by treating the bombarded layer as an effective continuum subject to swelling and plastic deformation. σ_L is therefore a macro-stress, and it will be dealt with in Section IV.

Since the injected helium concentration depends on the depth and time, all parameters in Eqs. (6) and (7), with the exception of γ, are functions of depth and time.

The area fraction A of intersected bubbles can be related to the bubble density, N_V, and to the swelling, S, if we make certain assumptions about the spacial arrangement of the bubbles. We consider two extreme cases.

First, suppose the bubbles form a cubic lattice, as occasionally observed, and that the intersection plane coincides with a bubble lattice plane. Then, the aerial density of bubbles, N_A, is related to the volumetric density by

$$N_V = N_A^{3/2} \quad . \tag{8}$$

As the second case, we consider a random arrangement of the bubbles, in which case [18]

$$N_A = N_V r \tag{9}$$

provided all intersected bubbles have about equal radius. The area fraction

$$A = \pi r^2 N_A \tag{10}$$

and the swelling

$$S = \frac{4\pi}{3} r^3 N_V \tag{11}$$

can now be related with the use of Eqs. (8) and (9). For a bubble lattice, one finds

$$A = (3\sqrt{\pi}/4)^{2/3} S^{2/3} = 1.209 S^{2/3}, \tag{12}$$

and for the random bubble arrangement, one obtains simply

$$A = \frac{3}{4} S. \tag{13}$$

Next, we relate the gas pressure in the bubbles to the helium concentration and the bubble density. This is accomplished by multiplying the gas law

$$p \frac{4\pi}{3} r^3 = mkT\, z(\rho,T) \tag{14}$$

with N_V and by introducing the helium/metal atom ratio

$$f_{He} = mN_V\Omega, \tag{15}$$

where Ω is the atomic volume of the metal atoms. In the following, it will be assumed that only a negligible fraction of the helium atoms is not in bubbles. f_{He} is then equal to the implanted helium concentration expressed in parts per metal atom. Equation (14) can then be written as

$$pS = f_{He}\, z(\rho,T)kT/\Omega \ . \tag{16}$$

From the balance equation (6), we can then finally obtain the micro-stress as given by

$$\frac{\bar{\sigma}_n}{\mu} = \{f_{He}\, z\, \frac{kT}{\mu\Omega} - \frac{2\gamma}{\mu}\,(4\pi N_v/3)^{1/3}\, S^{2/3}\}F(S)\ , \tag{17}$$

where

$$F(S) = \begin{cases} \dfrac{1.209}{S^{1/3} - 1.209S} & \text{for random bubbles} \\ \dfrac{1}{4/3 - S} & \text{for a bubble lattice}\ . \end{cases} \tag{18}$$

Equation (17) has been written as much as possible in terms of dimensionless parameters, such as the lattice strain $\bar{\sigma}_n/\mu$, the helium/metal atom ratio f_{He}, and γ/μ. The advantage for doing this is that γ/μ and T_m/μ are roughly equal for all metals; here T_m is the melting temperature. Therefore, the results given below are applicable to most metals including nickel which has been used as a typical representative.

In order to evaluate Eq. (17), we use Eqs. (11) and (15), and relate swelling to the implanted helium concentration, i.e.,

$$S = f_{He}/\rho \tag{19}$$

where ρ is the helium density in the bubbles. St-Jacques et al., [10] have recently measured the swelling during helium implantation into Nb and found that

$$S = (1.1 \pm 0.1)f_{He}\ .$$

This implies that the helium density in bubbles remains constant during the implantation at a ratio of about one helium atom per vacancy.

In general, however, ρ may change during the bombardment, so we have chosen a few values of ρ around one, and computed the lattice strain $\bar{\sigma}_n/\mu$ as a function of f_{He}. Typical results are shown in Figs. 3 and 4 for the case of nickel at T = 500 K and with a bubble density of 10^{17}cm^{-3}. It is

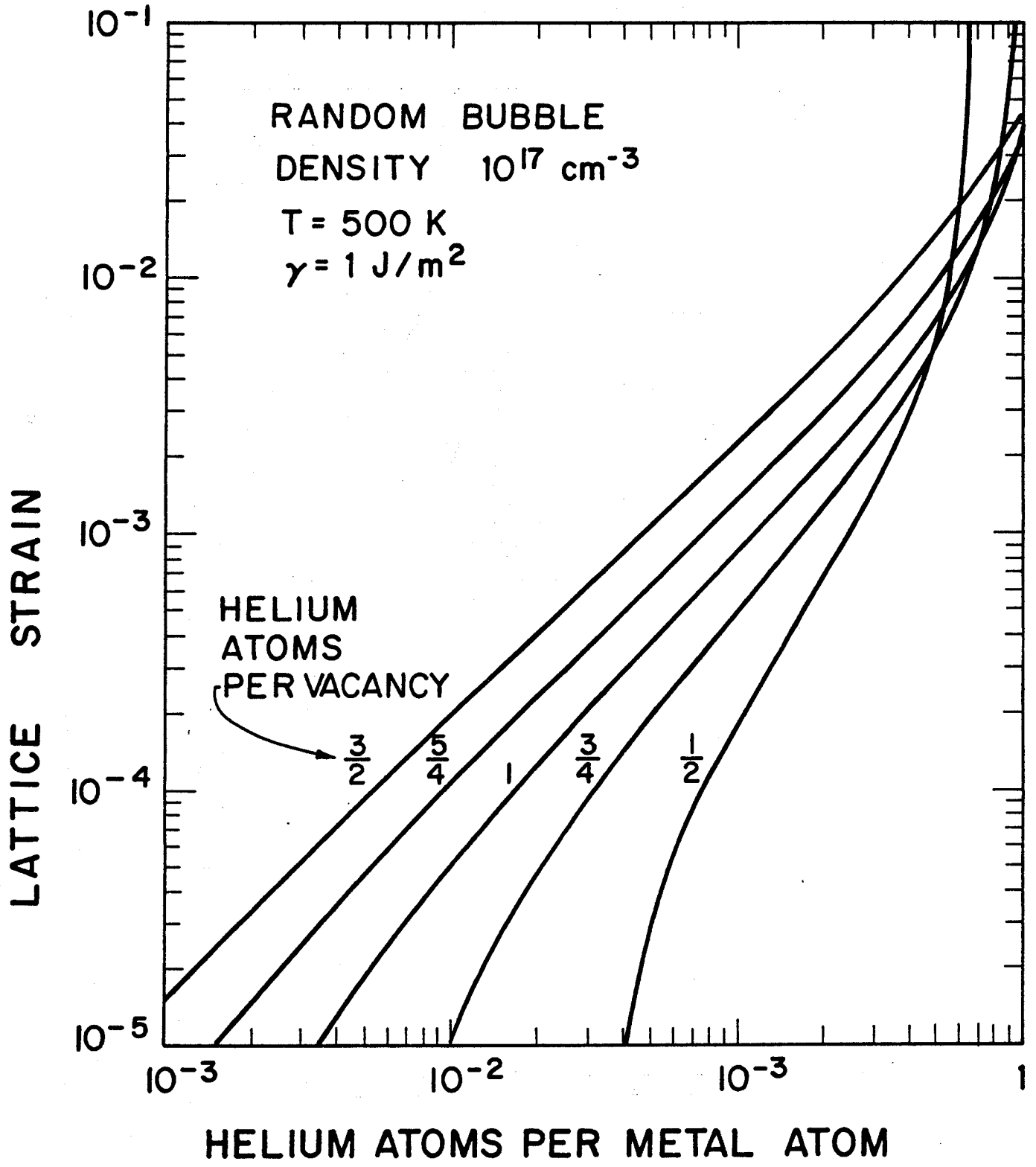

Fig. 3. Interbubble lattice strain for random bubble case as a function of the implanted helium concentration.

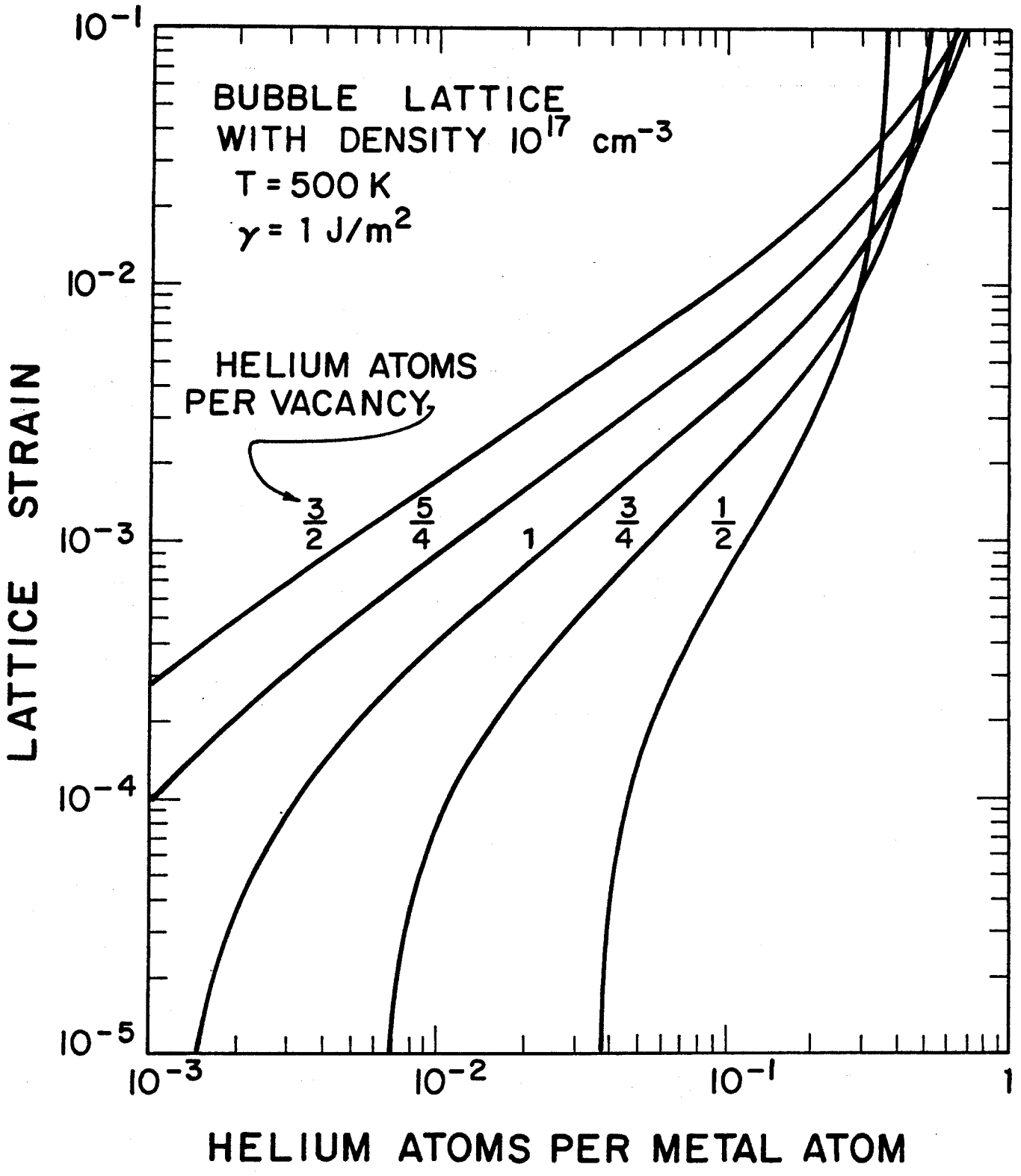

Fig. 4. Interbubble lattice strain for the bubble lattice as a function of the implanted helium concentration.

seen that the lattice strain in between bubbles steadily increases with the concentration of implanted helium, and rupture of the material becomes imminent.

In order to determine the critical helium concentration for rupture and blistering, we must define the fracture condition. Evans [5] has selected the ultimate theoretical strength of solids as the fracture criterion. We believe that this is much too high because failure of materials even at cryogenic temperatures occurs at a lower stress. According to the recent review on fracture mechanisms by Ashby and co-workers [19,20], the ultimate tensile strength determines both the ductile transgranular fracture of fcc metals, and the transgranular cleavage fracture of bcc and hcp metals. Therefore, the ultimate lattice strain for fcc materials is typically $\bar{\sigma}_n/\mu = 0.003$ [19], and for bcc materials three times larger [20]. Since bubble lattices are predominantly found in the bcc refractory metals, we select a failure stress of $\bar{\sigma}_n = 0.009\ \mu$ for the bubble lattice, and $\sigma_n = 0.003\ \mu$ for random bubble arrangement.

Critical helium concentrations at the onset of blistering, obtained in this manner, are shown in Figs. 5 and 6 as a function of the helium per vacancy ratio, and for bubble densities varying over two orders of magnitude. It is seen that the predicted critical helium concentration for $\rho = 1$ is around 20% to 40% of the metal atom density, in agreement with the experimental findings. In addition, however, the critical helium concentration is not strongly dependent on either the bubble density or the helium density in the bubbles as long as it is below the ratio of one helium atom per vacancy. The insensitivity to the bubble density implies that the surface tension plays a minor role in

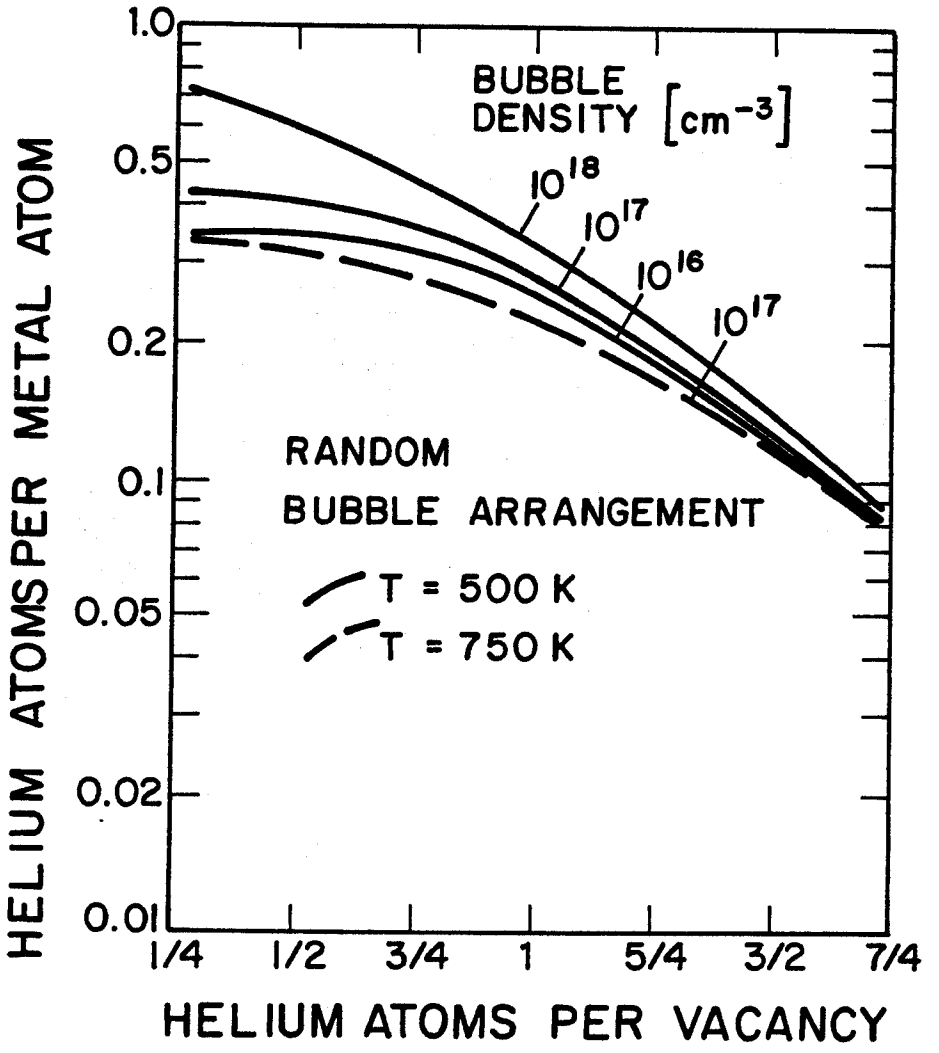

Fig. 5. Critical implanted helium concentration versus helium concentration in the bubbles. Case of random bubbles.

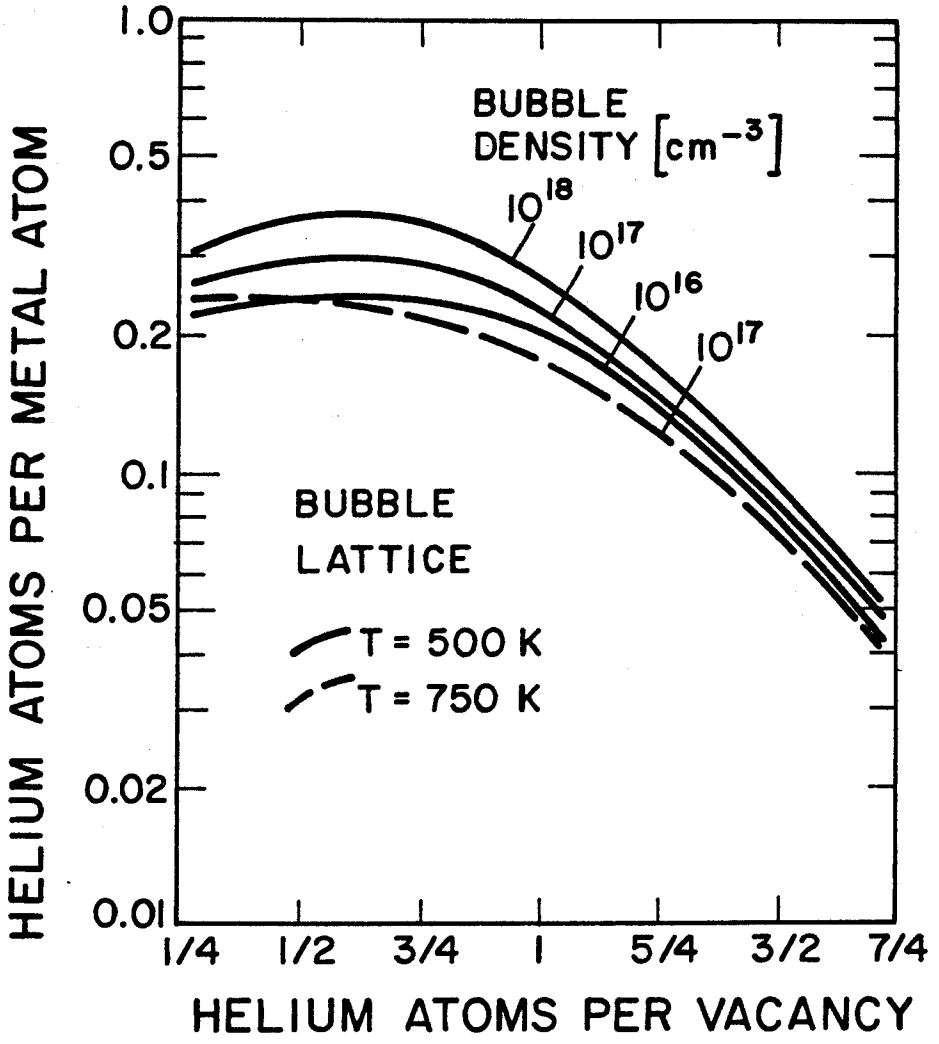

Fig. 6. Same as Fig. 5, but for the bubble lattice.

opposing the gas pressure. The weak dependence on the helium/vacancy ratio for values smaller than one can be explained as follows. As ρ decreases, the gas pressure is reduced, but at the same time, the load-carrying area (1-A) is also decreasing because the bubble volume goes up. As a result, $\bar{\sigma}_n/\mu$ remains roughly constant.

This conclusion would had been different if we had used a gas law with a fixed atomic diameter for helium. Then, the critical concentration would have been between 40% and 4% as ρ is increased from 1/4 to 1. It is therefore crucial to use an equation of state which accounts for the soft interatomic repulsion between helium. In other words, it is important to recognize that helium gas can be readily compressed at high temperature to liquid densities.

IV. Lateral Stresses Produced by Swelling

The swelling produced by the implanted gas is restrained in the lateral direction, i.e. parallel to the surface, because the thickness of the layer implanted is very small compared to the thickness of the entire sample. We may therefore approximate the real situation by a semi-infinite medium. The sum of all the strains, elastic, swelling, plus plastic, must then always remain zero in the lateral directions. For an isotropic material, the lateral stress components in two orthogonal directions are equal. Hooke's law for the elastic lateral strain in any given direction can be written as

$$E\varepsilon_L = (1-\nu)\sigma_L \tag{20}$$

where E is Young's modulus and ν is Poisson's ratio. The inelastic strain rate in the lateral direction is the sum of the swelling rate, $\dot{S}$, and the plastic deformation rate $\psi\sigma_L/3$. From the condition

$$\dot{\varepsilon}_L + \frac{1}{3}[\dot{S} + \psi\sigma_L] = 0 \tag{21}$$

follows with equation (20) that

$$\dot{\sigma}_L + \frac{E}{3(1-\nu)}[\dot{S} + \psi\sigma_L] = 0 \quad . \tag{22}$$

Assuming that $\dot{S}$ and ψ are independent of time and stress,

$$\sigma_L(t) = -(\dot{S}/\psi)[1 - \exp(-\frac{E\psi t}{3(1-\nu)})] \tag{23}$$

For a short time, $\sigma_L(t)$ can be approximated by

$$\sigma_L(t) \cong -\frac{E}{3(1-\nu)}\dot{S}t \tag{24}$$

and the stress builds up in proportion to the swelling. However, the increasing compressive stress eventually activates plastic deformation processes, and a saturation level is reached given by

$$\sigma_L(\infty) = -\dot{S}/\psi \quad . \tag{25}$$

This analysis is strictly valid only for irradiation creep, as it is linear in the stress. Thermally activated creep and plastic flow are highly nonlinear in their stress dependencies. Nevertheless, the above result remains qualitatively valid even for other deformation processes; namely, the stress rise is initially linear with swelling or helium fluence with a slope equal to $E/[3(1-\nu)]$, and later on follows a declining rate of increase. If plastic flow is the mechanism for stress relief, the stress versus swelling or helium fluence will look like a stress-strain curve in a compression experiment under constant strain rate. In this case, the maximum lateral stress is expected to be equal to the ultimate stress for compression.

If the irradiation creep rate were the controlling stress relief mechanism, then the maximum lateral stress would be given by Eq. (25). An estimate of its value for austenitic stainless steels can be obtained as follows.

The radiation damage accumulated at the onset of blistering is of the order of a 100 dpa. The irradiation creep strain rate over this dose range is estimated to be [21]

$$\dot{\varepsilon} \cong 0.12(\sigma/\mu)\text{dpa}^{-1} = \psi\sigma \tag{26}$$

for stainless steel irradiated at $T \lesssim 700$ K. Taking a value of 30% for swelling at the onset of blistering, we find according to Eq. (25) a maximum lateral stress of

$$\sigma_L \simeq -0.025\ \mu \tag{27}$$

which is about an order of magnitude higher than both the yield stress or the ultimate stress.

Irradiation creep is therefore not a significant stress relief mechanism, unless it is at least an order of magnitude larger for helium bombardment than for neutron bombardment. In any case, however, the lateral stress is expected to reach values of the order of the ultimate stress prior to the onset of blistering.

V. The Combined Role of the Stresses

As shown in the previous sections, gas bubble swelling generates both the microstress $\bar{\sigma}_n$ in between bubbles as well as the lateral macrostress σ_L. Whereas the direction of the latter is everywhere parallel to the surface, the former encircles the bubbles, so that the two superimpose as indicated in Fig. 2. On parallel intersection planes, the two stresses are orthogonal to each other and combine to give a maximum shear stress. Since failure is

due to plastic shear of the material in between bubbles, the lateral stress can contribute to the onset of blistering.

On the other hand, on perpendicular intersection planes, the two stresses are parallel and oppose each other. The magnitude of the net stress depends on the rate of stress relief for σ_L. At low temperatures where plastic flow or irradiation creep are the dominant deformation processes, σ_L is of the same order as $\bar{\sigma}_n$, and the two stresses nearly cancel each other.

At high temperatures, thermal creep provides an effective relief of the lateral stress, and σ_L is expected to be small. Contrary, $\bar{\sigma}_n$ is not relaxed by thermal creep. Although it promotes bubble swelling and thereby reduces the gas pressure, it reduces at the same time the load-carrying cross-section (1-A) of the material in between bubbles. Therefore, as mentioned earlier, $\bar{\sigma}_n$ remains nearly unchanged. At high temperatures, interbubble fracture can then also occur on perpendicular intersection planes. In this case, gas can be released to the surface without blistering. This may be a factor for the lack of blister formation at high temperatures.

The blisters that form at lower temperatures often assume the shape of spherical caps, and it is found that the diameter D of the blister base and its thickness t_b are related by

$$D \sim t_b^m \tag{28}$$

where m has been reported to be equal to 1.5 [22,23] or ranging from 0.85 to 1.25 depending on the metal [24]. The relationship (28) with m = 1.5 has been considered as strong evidence [8,22,23] that blistering is caused by the lateral stress, or rather by its integrated value, the compressive

load per unit length. As we have seen, the lateral stress reaches a saturation value prior to the onset of blistering. Therefore, the critical helium dose is clearly determined by the microstress $\bar{\sigma}_n$.

The blister formation must then be considered as a two-stage process: decohesion of the bombarded layer starts at the depth, t_b, of maximum $\bar{\sigma}_n$. Once initiated, the penny-shaped crack that forms spreads until a diameter D is reached where the buckling condition [23]

$$D = 1.55 \left[\frac{\mu}{(1-\nu)P}\right]^{1/2} t_b^{3/2} \tag{29}$$

is satisfied for the already existing lateral load

$$P = - \int_0^{t_b} \sigma_L \, dt_b \quad . \tag{30}$$

Some refinement of this simple buckling model may be desirable to include a gradient of σ_L, i.e., a bending moment, as well as connecting ligaments between the otherwise detached layer and the underlying material. It is expected that these refinements will give values of m somewhat different from the classical value of 1.5.

In summary, our analysis of the role of gas pressure and lateral stress essentially confirms the major conclusion reached by Evans [5], namely that the gas pressure in bubbles is the prime initiator of blistering. However, in contrast to Evans, we assign the lateral stress a significant role in the formation of the blister domes. Furthermore, the laterial stress is also the driving force for the extrusion of the swelling layer in the direction perpendicular to the specimen surface.

Acknowledgement

Most of this research was carried out at the Institute for Plasma Physics, Garching, Germany, during the summer of 1979. The author gratefully acknowledges the hospitality of the Institute as well as fruitful discussions with Drs. Behrisch, Roth, and Scherzer.

References

1. S. K. Das and M. Kaminsky, in Radiation Effects on Solid Surfaces, ed. by M. Kaminsky, Adv. in Chemistry Series, Vol. 158, Am. Chem. Soc., Wash., 1976, Ch. 5.

2. B. M. U. Scherzer, to be published.

3. W. D. Wilson and R. A. Johnson, in Interatomic Potentials and Simulation of Lattice Defects, ed. by P. C. Gehlen, J. R. Beeler and R. I. Jaffee, Plenum Press, 1972, p. 375.

4. W. D. Wilson, C. L. Bisson, and D. W. Amos; J. Nucl. Materials 53 (1974), 154.

5. J. H. Evans, J. Nucl. Materials 76 & 77 (1978), 228.

6. W. G. Wolfer, to be published.

7. R. Behrisch, J. Bottinger, W. Eckstein, U. Littmark, J. Roth, and B. M. U. Scherzer; Appl. Phys. Letters 27 (1975), 199.

8. E. P. EerNisse and S. T. Picraux, J. Appl. Phys. 48 (1977), 9.

9. R. G. St-Jacques, G. Veilleux, J. G. Martel, and B. Terreault; Proc. Internat. Conf. on Ion Beam Modification of Materials, Budapest, 1978.

10. R. G. St-Jacques, G. Veilleux, and B. Terreault; 8th Internat. Conf. on Atomic Collisions in Solids, Hamilton, Canada, 1979.

11. W. G. Wolfer and F. A. Garner; J. Nucl. Materials 85 & 86 (1979), 583.

12. R. D. McCarthy; J. Phys. Chem. Ref. Data 2 (1973), 924.

13. D. E. Beck; Molec. Phys. 14 (1968), 311.

14. J. A. Barker and D. Henderson; Rev. Mod. Phys. 48 (1976), 587.

15. H. C. Anderson, D. Chandler, and J. D. Weeks; Adv. Chem. Phys. 34 (1976), 105.

16. L. Verlet and J. J. Weis; Phys. Rev. A5 (1972), 439; Molec. Phys. 24 (1972), 1013.

17. See, e.g., R. G. Lindford, "Surface Thermodynamics of Solids," ch. 1 in Solid State Surface Science, Vol. 2, ed. by M. Green, Marcel Dekker, N.Y., (1972).

18. E. E. Underwood, Quantitative Stereology, Addison-Wesley, Reading, (1970).

19. M. F. Ashby, C. Gandhi, and D. M. R. Taplin; Acta Met. 27 (1979), 699.

20. C. Gandhi and M. F. Ashby; Acta Met. 27 (1979), 1565.

21. W. G. Wolfer; J. Nucl. Materials, to appear.

22. J. Roth, Appl. of Ion Beams to Materials, ed. G. Carter, J. S. Colligon, and W. A. Grant, The Institute of Phys., London (1976), 280.

23. M. Risch, J. Roth, and B. M. U. Scherzer, Plasma Wall Interaction, Proc. Intl. Symp., Pergamon, Oxford and New York (1977), 391.

24. S. K. Das, M. Kaminsky, and G. Fenske, J. Nucl. Materials 76 & 77 (1978), 255.